ACS APPLIED MATERIALS & INTERFACES

Research Article

www.acsami.org

New Ce^{3+}-Activated Thiosilicate Phosphor for LED Lighting—Synthesis, Luminescence Studies, and Applications

Szu-Ping Lee,[†] Chien-Hao Huang,[‡] Ting-Shan Chan,[§] and Teng-Ming Chen*,[†]

[†]Phosphors Research Laboratory, Department of Applied Chemistry and Institute of Molecular Science, National Chiao Tung University, Hsinchu 30010, Taiwan

[‡]Material and Chemical Research Laboratories, ITRI, Hsinchu 30011, Taiwan

[§]National Synchrotron Radiation Research Center, Hsinchu 30076, Taiwan

Supporting Information

ABSTRACT: A new Ce^{3+}-activated thiosilicate phosphor, $BaLa_2Si_2S_8:Ce^{3+}$, was synthesized by using solid-state methods in a fused silica ampule and found to crystallize in the structure type of $La_2PbSi_2S_8$. The crystal structure has been characterized by synchrotron X-ray diffraction and refined with Rietveld methods. This novel cyan-emitting phosphor can be excited over a broad range from UV to blue light (380−450 nm) and generates a broadband emission peaking at 471 nm with a quantum efficiency of 36%. Nonradiative transitions between Ce^{3+} ions in $BaLa_2Si_2S_8:Ce^{3+}$ have also been demonstrated to be attributable to dipole−dipole interactions, and the critical distance was calculated to be 17.41 Å. When $BaLa_2Si_2S_8:Ce^{3+}$ phosphor was utilized to incorporate with yellow-emitting $(Sr,Ca)_2SiO_4:Eu^{2+}$ phosphor and red-emitting $CaAlSiN_3:Eu^{2+}$ phosphor on a 430 nm blue LED chip, a warm white light LED device with color rendering index of ∼96 was obtained. The results indicate that cyan-emitting $BaLa_2Si_2S_8:Ce^{3+}$ can serve as a potential phosphor for incorporation in fabrication of solid-state lighting. The preparation, spectroscopic characterization, quantum efficiency, decay lifetime, thermal-quenching behavior, and related LED device data are also presented.

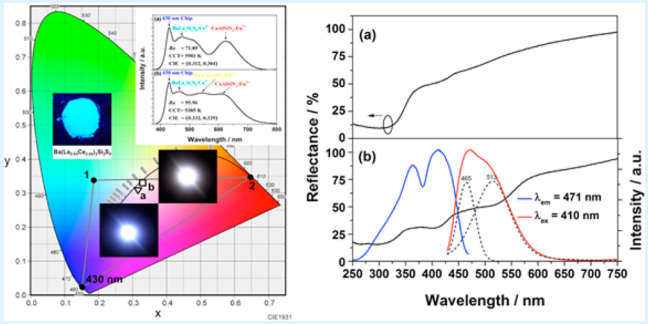

KEYWORDS: *$BaLa_2Si_2S_8:Ce^{3+}$, thiosilicate phosphor, photoluminescence, white-light LED*

INTRODUCTION

Since the invention of the blue light-emitting InGaN-based light emitting diode (LED) in the early 20th century, remarkable progress has been made in the development of commercially realized efficient white light LEDs (WLEDs).[1,2] By the combination of blue emission from the InGaN-based LED chips and yellow emission from the down-conversion of $Y_3Al_5O_{12}:Ce^{3+}$ (YAG:Ce)-based phosphors,[3] the generated white light has already exceeded that of incandescent lamps and is competitive with conventional fluorescent lamps.[4,5] WLEDs are energy-efficient, life-durable, and environmentally friendly in comparison to conventional light sources; however, the color quality of WLEDs still requires improvement with respect to tunability of the white hue, color temperature, and color rendering.[6] In particular, these properties are closely correlated to the general illumination.[7,8] For most of the currently applied phosphors in the WLEDs system, they do not reach the optimal requirements for white light and show poor color rendition in the red spectral region.[9,10] Therefore, to attain the optical requirements for white light, many new phosphors are reported in order to overcome the aforementioned drawbacks and to obtain suitable luminescent material for phosphor-converted white light emitting diodes (pc-WLEDs).[6,11]

The luminescence properties of binary $A^{II}S$ (A = Ca, Sr, Ba, Zn)[12,13] and ternary $A^{II}B^{III}{}_2S_4$ (B = Al, Ga, In)[14,15] sulfide compounds doped with various transition metals (such as Cu, Ag, and Pb) or rare earth ions (Ce^{3+} and Eu^{2+}) have been investigated for more than thirty years. These compounds have attracted significant interest due to their capability for lighting and display applications.[16,17] Moreover, many studies have reported the photoluminescence (PL) characteristics of sulfide phosphors for compensating the red color deficiency and producing high color rendering white light in the WLEDs.[18] Recently, some luminescent oxysulfide-based phosphors have been developed; Kuo et al. reported that the $CaZnOS:Eu^{2+}$[19] phosphor exhibits a broad absorption band and excellent color purity as a complementary red-emitting component. Yu et al. presented the luminescence properties of the $CaAl_2S_4:Eu^{2+}/Ce^{3+}$ thioaluminate phosphor.[20] Parmentier et al. reported a new family of $M_2SiS_4:Eu^{2+}$ (M = Ca, Sr, and Ba)[21] thiosilicate

Received: January 24, 2014
Accepted: April 25, 2014
Published: April 25, 2014

   dx.doi.org/10.1021/am500483j | ACS Appl. Mater. Interfaces 2014, 6, 7260−7267

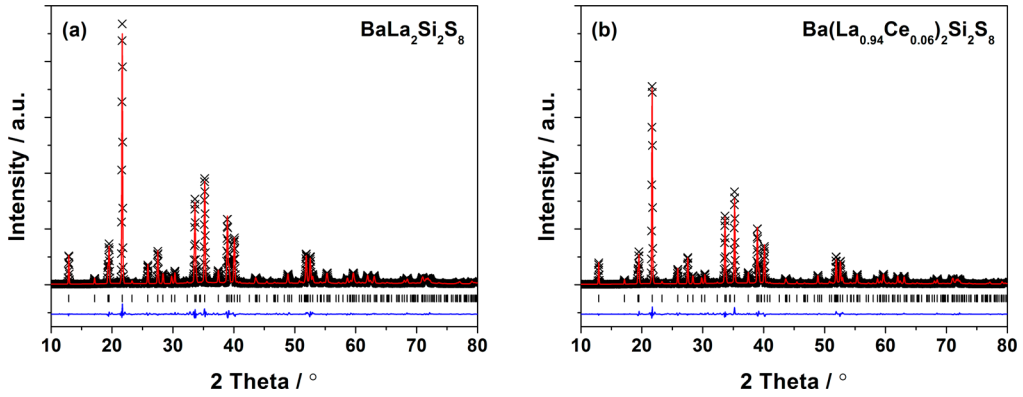

Figure 1. SXRD profiles for Rietveld refinement results of (a) $BaLa_2Si_2S_8$ and (b) $Ba(La_{0.94}Ce_{0.06})_2Si_2S_8$. Observed intensities (cross), calculated patterns (red line), Bragg positions (tick mark), and difference plot (blue line) are presented.

phosphors and its tunable PL characteristics by adjusting the alkaline earth ratio. Although sulfide phosphors have met with a predicament in terms of rapid degradation of luminescent intensity because of a relatively unstable thermal chemical property when compared to oxides, the low manufacturing temperature and superior optical variety still make sulfides attractive.

For most phosphors doped with Ce^{3+}, a parity-allowed 5d−4f emission ranging from ultraviolet to red color is shown depending upon the host lattice and the site size, site symmetry, and coordination number. In fact, the emission color of Ce^{3+} can also be controlled in the desired region of the spectrum by changing the crystal field strength.[22−24] For example, the optical properties of Ce^{3+} dopant in $Ca(Si,Al)N_2:Ce^{3+}$ (red),[25] $(La,Gd)Sr_2AlO_5:Ce^{3+}$(yellow),[26] and $(Ca,Sr)Sc_2O_4:Ce^{3+}$ (green)[27] phosphors have been investigated. In this research, we have discovered and report a new Ce^{3+}-activated $BaLa_2Si_2S_8$ thiosilicate phosphor, which was found to crystallize in the structure type of $La_2PbSi_2S_8$.[28] For the first time, we investigated the crystal structure of $BaLa_2Si_2S_8$ lattice obtained from Rietveld refinement via synchrotron X-ray diffraction (SXRD) patterns and reported the luminescent properties of the $BaLa_2Si_2S_8:Ce^{3+}$ phosphor. This new phosphor can be excited by light in the n-UV to blue region and shows cyan emission. In addition, the temperature dependence of the LED device using $BaLa_2Si_2S_8:Ce^{3+}$ phosphor with a blue LED chip was investigated to demonstrate the applicability of the $BaLa_2Si_2S_8:Ce^{3+}$ phosphor as a color conversion material.

EXPERIMENTAL SECTION

Materials. The powder samples of $Ba(La_{1-x}Ce_x)_2Si_2S_8$ were synthesized by solid-state reactions using La_2S_3 (Alfa, 99%), BaS (Alfa, 99.7%), Ce_2S_3 (Alfa, 99.99%), Si powder (Alfa, 99.999%), and S powder (Acros, 99.999%) as raw materials. The stoichiometric amounts of the starting materials were thoroughly mixed and loaded into a vertically positioned fused silica ampule, fully evacuated to 10^{-3} Torr, and sealed off under a dynamic vacuum. The fused silica ampule was heated at 5 °C/min to 1000−1100 °C for 6−8 h in a furnace and then cooled down slowly to room temperature. The chemical reaction can be summarized in the following:

$$BaS + (1 - x)La_2S_3 + xCe_2S_3 + 2Si + 4S \rightarrow Ba(La_{1-x}Ce_x)_2Si_2S_8 \quad (1)$$

The pc-WLEDs devices were fabricated using commercial blue InGaN-based LEDs (λ_{max} = 430 nm) with an intimate mixture of silicone resin and phosphor blending of cyan-emitting $BaLa_2Si_2S_8:Ce^{3+}$, yellow-emitting $(Sr,Ca)_2SiO_4:Eu^{2+}$[29] commodity (Intematix-Y4453), and red-emitting $CaAlSiN_3:Eu^{2+}$[30] commodity (Mitsubishi-BR-102C) in the ratio of 6:3:2.

Characterization. SXRD profiles were recorded at the BL01C2 beamline of National Synchrotron Radiation Research Center (NSRRC) in Hsinchu, Taiwan, equipped with a Mar345 imaging plate and using an X-ray wavelength of 0.774908 Å. X-ray Rietveld refinements were conducted using the General Structure Analysis System (GSAS) software.[31,32] The morphology and energy-dispersive X-ray spectroscopy (EDS) spectrum were measured by a JEOL JSM-7401F conventional thermal field-emission scanning electron microscope. The diffuse reflection (DR) spectra were measured with a Hitachi 3010 double-beam UV−vis spectrometer (Hitachi Co., Tokyo, Japan) equipped with a ø60 mm integrating sphere. The photoluminescence (PL) and photoluminescence excitation (PLE) spectra were recorded with a Spex Fluorolog-3 spectrofluorometer (Jobin Yvon Inc./Specx) equipped with a 450 W Xe lamp and analyzed by a Jobin-Yvon spectrometer HR460 with multichannel charge-coupled device detector. The luminescence decay lifetime were measured on a tunable nanosecond optical-parametric-oscillator/Q-switch-pumped YAG:Nd^{3+} laser system (Ekspla). The quantum efficiency (QE) was measured by an integrating sphere whose inner face was coated with Spectralon equipped with a spectrofluorometer (Horiba Jobin-Yvon Fluorolog 3−2−2). The thermal luminescence (TL) quenching was tested using a heating apparatus (THMS-600) in combination with PL equipment. The Commission Internationale de l'Eclairage (CIE) chromaticity coordinates were determined by a Laiko DT-100 color analyzer equipped with a CCD detector (Laiko Co., Tokyo, Japan). The electroluminescence (EL) spectra were recorded under a forward bias current 350 mA and measured by using a SphereOptics integrating sphere with LED measurement starter packages (Onset, Inc.).

RESULTS AND DISCUSSION

Structural Characterizations and Crystallographic Parameters of the $BaLa_2Si_2S_8$ and $Ba(La_{0.94}Ce_{0.06})_2Si_2S_8$ Phosphors. To approach a dependable approximation of the actual crystal structure, the isotypic single-crystal structure data of $La_2PbSi_2S_8$ were used as a starting model.

$LaPb_2Si_2S_8$ is reported with crystallographic data by Gulay et al.[28] With the similar size of ionic radii in eightfold coordinated Pb^{2+} ion and alkaline-earth metal(II), such as Ba^{2+} ion,[33] we can demonstrate the adaptability of a new phosphor host $BaLa_2Si_2S_8$.

The Rietveld refinements are accomplished for $BaLa_2Si_2S_8$ and $Ba(La_{0.94}Ce_{0.06})_2Si_2S_8$ phosphors from the observed SXRD patterns (Figure 1) and show that the final converged weighted profiles of R_{wp} are 9.18% and 8.77%, respectively, indicating the single phase with no unidentified diffraction peaks from impurity. Both structures are found to crystallize hexagonally

dx.doi.org/10.1021/am500483j | ACS Appl. Mater. Interfaces 2014, 6, 7260−7267

Table 1. Structural Parameters of $BaLa_2Si_2S_8$ and $Ba(La_{0.94}Ce_{0.06})_2Si_2S_8$ of Rietveld Refinement from SXRD Data at Room Temperature[a]

formula		$BaLa_2Si_2S_8$					$Ba(La_{0.94}Ce_{0.06})_2Si_2S_8$				
density		3.640 (g/cm^3)					3.647 (g/cm^3)				
lattice parameters		a = 918.109(20), c = 2729.41(7), V =1992.27(8)					a = 917.344(16), c = 2729.16(6), V = 1989.12(7)				
R_{wp}		9.18%					8.77%				
R_p		6.34%					6.09%				
χ^2		2.509					1.740				
atom	Wyck.	x/a	y/b	z/c	S.O.F	U_{iso}*100	x/a	y/b	z/c	S.O.F	U_{iso}*100
Ba	18e	0.34606(16)	0.01273(16)	0.0833	0.333	5.55(6)	0.34628(16)	0.01296(16)	0.0833	0.333	5.44(6)
La	18e	0.34606(16)	0.01273(16)	0.0833	0.667	5.55(6)	0.34628(16)	0.01296(16)	0.0833	0.627	5.44(6)
Si	12c	0.6667	0.3333	−0.0055(4)	1.000	5.43(30)	0.6667	0.3333	−0.00596(35)	1.000	5.57(29)
S1	12c	0.3333	−0.3333	0.08452(33)	1.000	4.92(25)	0.3333	−0.3333	0.08449(31)	1.000	5.18(24)
S2	36f	0.4348(5)	0.3009(5)	0.01937(14)	1.000	5.19(18)	0.4347(4)	0.3012(5)	0.01945(14)	1.000	4.95(17)
Ce	18e						0.34629(16)	0.01296(16)	0.0833	0.040	5.44(6)

[a]Hexagonal; space group: $R\bar{3}c$ (No. 167); lattice parameters: a and c in pm, V in 10^6 pm^3; U_{iso} in Å^2; $\alpha = \beta = 120°$, $\gamma = 90°$; T = 298 K; Z = 6; beamline 01C2 of NSRRC, λ = 0.77491 Å; Site Occupancy Fraction (S.O.F.).

in space group: $R\bar{3}c$ (No. 167) with Z = 6. In the crystal lattice and the unit cell of $BaLa_2Si_2S_8$, there are a single site (18e) randomly occupied by a mixture of the Ba and La atoms, one site of the Si atoms, and two sites of the chalcogen atoms. The sites of the Si and S atoms are fully occupied. For each material, by treating the 18e site occupancy factor as a free parameter, it has been refined to a numerical value close to 1/3Ba + 2/3La.[34] Compared to $BaLa_2Si_2S_8$, the parameters and the bond distances of the $Ba(La_{0.94}Ce_{0.06})_2Si_2S_8$ lattice were found to decrease with increasing Ce^{3+} dopant content because of the smaller ionic radius of cerium ions. The fractional occupancies of each component atom are adjusted to the nominal stoichiometry. The final refined structural parameters, selected atomic distances, and bond angles of $BaLa_2Si_2S_8$ and $Ba(La_{0.94}Ce_{0.06})_2Si_2S_8$ are summarized in Table 1 and Table 2,

Table 2. Selected Interatomic Bond Distances[a] of $BaLa_2Si_2S_8$ and $Ba(La_{0.94}Ce_{0.06})_2Si_2S_8$ at Room Temperature

$BaLa_2Si_2S_8$		$Ba(La_{0.94}Ce_{0.06})_2Si_2S_8$	
(Ba/La)-S1	312.06(8) (2×)	(Ba/La/Ce)-S1	311.91(8) (2×)
(Ba/La)-S2	292.55(4) (2×)	(Ba/La/Ce)-S2	292.35(4) (2×)
(Ba/La)-S2^{i}	334.45(4) (2×)	(Ba/La/Ce)-S2^{i}	333.8(4) (2×)
(Ba/La)-S2^{ii}	304.7(4) (2×)	(Ba/La/Ce)-S2^{ii}	304.8(4) (2×)
(Ba/La)-Si	381.4(6) (2×)	(Ba/La/Ce)-Si	381.1(6) (2×)
(Ba/La)-Si^{i}	377.5(6) (2×)	(Ba/La/Ce)-Si^{i}	376.7(5) (2×)

[a]Bond distances in pm.

respectively. The grain size and morphology of $Ba(La_{0.94}Ce_{0.06})_2Si_2S_8$ particles were characterized by SEM, which indicates that the as-synthesized phosphor was composed of many irregular granular microcrystals. The nominal stoichiometry was also verified by EDS spectrum (see Figure S1 in the Supporting Information (SI)).

Figure 2 shows the exact crystal structure of $BaLa_2Si_2S_8$ lattice viewed along the c- axis and Ba/La atomic site with their corresponding neighboring atoms from the refined results. Generally, the atomic framework consists of [(1/3Ba + 2/3La)S_8] bicapped trigonal prisms and [SiS_4] tetrahedra, which are mutually connected by corners and edges.[34] The coordination polyhedron of Ba/LaS_8 is composed of eight S and one Ba/La atoms situated in the center of the bicapped trigonal prism with CN of 8.

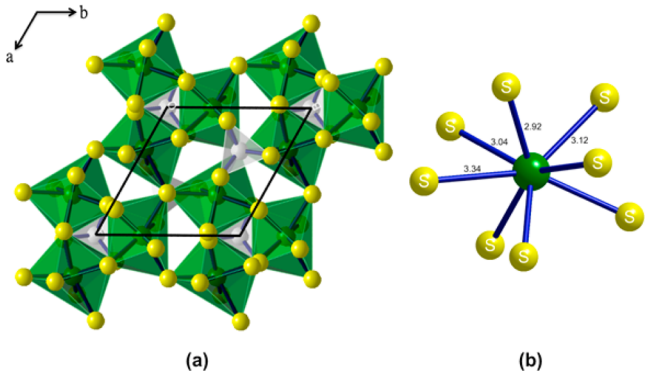

Figure 2. (a) Schematic unit cell crystal structure of $Ba(La_{0.94}Ce_{0.06})_2Si_2S_8$ viewed along the c axis and (b) coordination environment around Ba/LaS_8. Green, yellow, and white sphere balls describe Ba/La/Ce, S, and Si atoms.

Spectroscopic Study of the $Ba(La_{1-x}Ce_x)_2Si_2S_8$ Thiosilicate Phosphor. Figure 3 shows the DR spectrum of as-synthesized polycrystalline $BaLa_2Si_2S_8$ and $Ba(La_{0.94}Ce_{0.06})_2Si_2S_8$. For the $BaLa_2Si_2S_8$ host, the DR spectrum shows a status of high reflection in the wavelength ranging from

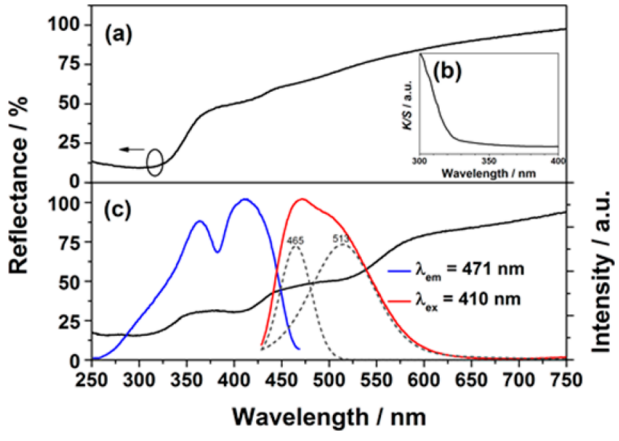

Figure 3. (a) DR spectrum of $BaLa_2Si_2S_8$ host. (b) Kubelka–Munk absorption spectrum for $BaLa_2Si_2S_8$ host. (c) DR spectrum, PLE/PL spectra, and the PL deconvolution (dashed line) of $Ba(La_{0.94}Ce_{0.06})_2Si_2S_8$.

dx.doi.org/10.1021/am500483j | ACS Appl. Mater. Interfaces 2014, 6, 7260−7267

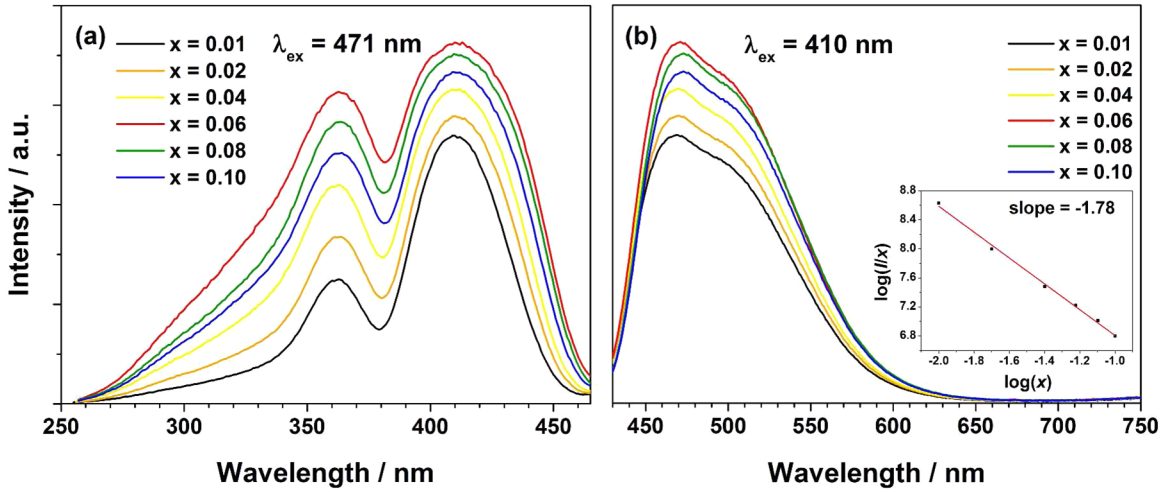

Figure 4. (a) PLE spectra (monitored at λ_{em} = 471 nm) and (b) PL spectra (λ_{ex} = 410 nm) of $Ba(La_{1-x}Ce_x)_2Si_2S_8$ with different Ce^{3+} concentration x. The inset shows the correlation between $\log(I/x)$ with $\log(x)$.

400 to 750 nm, and decreases intensely from 250 to 450 nm. The Kubelka–Munk absorption coefficient (K/S) relation is used to calculate the measured reflectance (R) for the host lattice (Figure 3b).[35]

$$\frac{K}{S} = \frac{(1-R)^2}{2R} \tag{2}$$

where K represents the absorption coefficient, S the scattering coefficient, and R the reflectivity. The fundamental band gap energy (absorption edge) of the $BaLa_2Si_2S_8$ host was calculated to be approximately 3.77 eV from the K/S relation spectrum. When 6% Ce^{3+} was introduced into the $BaLa_2Si_2S_8$ host lattice, the absorption edge extends to a longer wavelength side and the absorption is enhanced. The observed results suggest two different absorption pathways from UV to visible range, namely, one is caused by $BaLa_2Si_2S_8$ host and the other is caused by the $4f^1-5d^1$ transitions of Ce^{3+} ion.[36] A typical PLE/PL spectrum of $Ba(La_{0.94}Ce_{0.06})_2Si_2S_8$ is indicated in Figure 3b. The asymmetric emission band in the PL spectrum is fitted into a good approximation with two Gaussian curves centered, respectively, at 465 nm (21,505 cm^{-1}) and 513 nm (19,493 cm^{-1}), which can be ascribed to the transitions from the lowest 5d level to the two $^2F_{7/2}$ and $^2F_{5/2}$ ground states of the Ce^{3+} ions.[37] Then, the energy gap between $^2F_{7/2}$ and $^2F_{5/2}$ associated with spin–orbit coupling was calculated to be 2012 cm^{-1} (249 meV). On the other hand, the PLE spectrum is characterized by two main excitation bands in the UV–vis range: one band in the UV peaking at ~365 nm (ranging from 250 to 380 nm) and another band in the visible at ~410 nm (range from 380 to 460 nm). The PLE and PL spectra of $Ba(La_{1-x}Ce_x)_2Si_2S_8$ (x = 0.01, 0.02, 0.04, 0.06, 0.08, and 0.10) are shown in Figure 4a,b, respectively. The relative intensity in both PLE and PL spectra varies with different Ce^{3+} dopant concentrations, and an optimal value of x = 0.06 (ca. 6 mol %) is obtained for so-called critical concentration (x_c). Because each activator ion is introduced solely into one site, there is, on the average, one activator per V/x_cN when considering the concentration quenching caused by the energy transfer mechanisms, such as exchange interaction, radiation reabsorption, or multipole–multipole interaction.[38] The critical energy transfer distance (R_c) is approximately equal to twice the radius of a sphere with the volume.[38,39]

$$R_c \approx 2\left(\frac{3V}{4\pi x_c N}\right)^{1/3} \tag{3}$$

where V represents the volume of unit cell, x_c the critical dopant concentration, and N the number of total Ce^{3+} sites in the unit cell. In this case, V = 1989.13 Å^3, N = 6, and x_c = 0.12 (ca. 6 mol %). Thus, the R_c of Ce^{3+} was calculated to be 17.41 Å. If the rapid migration of Ce^{3+} ion happens, quenching tends to be proportional to the Ce^{3+} concentration, which is not being observed in PL spectra. Since the exchange interaction takes place generally in the forbidden transition (the R_c is typically ~5 Å), the PLE and PL spectra do not overlap very well. Therefore, we can infer that the nonradiative concentration quenching between two nearest Ce^{3+} centers occurs via electric multipolar interactions based on the Dexter theory.[40] For the emission intensity per activator concentration, the following equation can be described[41]

$$\frac{I}{x} = \frac{k}{1+\beta(x)^{\theta/3}} \tag{4}$$

where I represents the quenching intensity; x represents Ce^{3+} concentration; k and β represent constants for individual electric multipolar interactions; θ = 6, 8, and 10 demonstrate, respectively, the dipole–dipole, dipole–quadrupole, and quadrupole–quadrupole interations. As represented in Figure 4b, the correlation between $\log(I/x)$ with $\log(x)$ can be fitted linearly within PL spectra of $Ba(La_{1-x}Ce_x)_2Si_2S_8$ (x = 0.01, 0.02, 0.04, 0.06, 0.08, and 0.10) and the value θ was determined to be 5.34 from the slope ($\theta/3$). In particular, the calculated value for $Ba(La_{1-x}Ce_x)_2Si_2S_8$ is close to 6, which implies that the concentration quenching mechanism in Ce^{3+} emission is strongly accounted for by the dipole–dipole interaction. With increasing Ce^{3+} concentration, the wavelengths of excitation and emission bands remain practically unchanged for the phosphor material. In addition, the optical absorbance (φ) and quantum efficiency (η) were calculated by using the following equations:[42,43]

$$\varphi = \frac{L_o(\lambda) - L_i(\lambda)}{L_o(\lambda)} \tag{5}$$

dx.doi.org/10.1021/am500483j | ACS Appl. Mater. Interfaces 2014, 6, 7260–7267

$$\eta = \frac{E_i(\lambda) - (1-\varphi)E_o(\lambda)}{L_e(\lambda)\varphi} \quad (6)$$

where $L_o(\lambda)$ is the integrated excitation profile when the sample is diffusely illuminated by the integrated sphere's surface, $L_i(\lambda)$ is the integrated excitation profile when the sample is directly excited by the incident beam, $E_i(\lambda)$ is the integrated luminescence of the sample upon direct excitation, $E_o(\lambda)$ is the integrated luminescence of the sample excited by indirect illumination from the sphere, and $L_e(\lambda)$ is the integrated excitation profile obtained from the empty integrated sphere (without the sample present). As a result, $Ba(La_{0.94}Ce_{0.06})_2Si_2S_8$ exhibits quantum efficiency (η) values 36.07% under 410 nm and 30.39% under 430 nm excitation, which reflect the applicability for color conversion of white LED consisting of n-UV or blue chip. The full width at half-maximum (fwhm) of the emission band is found to be larger than 150 nm (66,667 cm^{-1}). These results depict that Ce^{3+}-doped $BaLa_2Si_2S_8$ thiosilicate phosphor may achieve good color rendering when incorporated into pc-WLEDs.

Temperature-Dependent PL Properties and Decay Lifetime of the $Ba(La_{1-x}Ce_x)_2Si_2S_8$ Thiosilicate Phosphor. Figure 5 shows the temperature-dependent PL spectra of

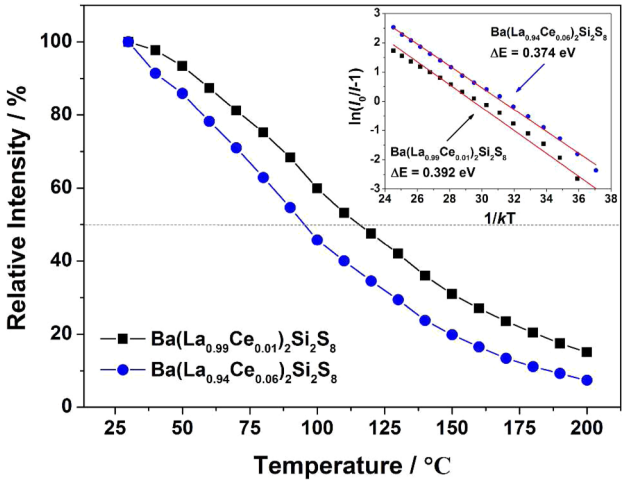

Figure 5. Temperature-dependent PL intensity of $Ba(La_{0.99}Ce_{0.01})_2Si_2S_8$ and $Ba(La_{0.94}Ce_{0.06})_2Si_2S_8$. The inset shows the fitted PL intensity and the calculated thermal activation energy (ΔE) as a function of temperature.

$Ba(La_{0.99}Ce_{0.01})_2Si_2S_8$ and $Ba(La_{0.94}Ce_{0.06})_2Si_2S_8$ in the range of 30 to 200 °C. The PL intensities of both samples are found to be diminished as compared to that of the same sample observed at room temperature, which may be rationalized by the fact that increasing temperature increases the population of higher vibration levels, the density of phonons, and the probability of nonradiative transfer.[44] In spite of the introduction of Si ions into the sulfide host, the $BaLa_2Si_2S_8$:Ce^{3+} does not show a stronger thermal stability than that of the commodity CaS:Ce^{3+}. To investigate the origin of temperature dependent emission intensity, the activation energy (E_a) of the electrons being excited from the 4f level to the lowest 5d level of Ce^{3+} can be described in following equation:[44]

$$I(T) = \frac{I_0}{1 + A\exp\left(-\frac{E_a}{kT}\right)} \quad (7)$$

where I_0 and $I(T)$ represent the PL intensity at room temperature and testing temperature (30–200 °C), respectively, and k the Boltzmann constant. The values of E_a for $Ba(La_{0.99}Ce_{0.01})_2Si_2S_8$ and $Ba(La_{0.94}Ce_{0.06})_2Si_2S_8$ were estimated to be 0.392 and 0.374 eV, respectively, as shown in the inset in Figure 5. With increasing Ce^{3+} concentration, the thermal energy was found to decrease and could excite the 5d electron to the bottom of the conduction band more easily.[36] In addition, for application in higher-powered LEDs, chemical stability of a phosphor is an important parameter to consider. Figure S2 in the SI presents the time-dependent PL intensity of $Ba(La_{0.94}Ce_{0.06})_2Si_2S_8$ exposed to ambient air. The PL intensity of $Ba(La_{0.94}Ce_{0.06})_2Si_2S_8$ drops only ~25% when exposed to ambient air for 5 weeks. This observation can illustrate that the $BaLa_2Si_2S_8$:Ce^{3+} thiosilicate phosphor is mostly stable against degradation in ambient condition.

Furthermore, the decay curves of $Ba(La_{1-x}Ce_x)_2Si_2S_8$ (x = 0.01, 0.06, and 0.10) phosphors excited at 420 nm and monitored at 471 nm are shown in Figure 6 and Figure S3 in

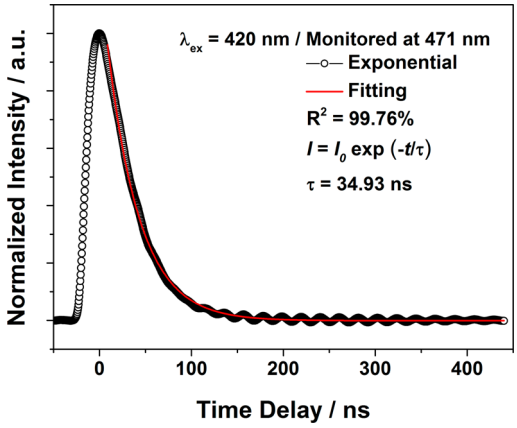

Figure 6. Decay curve for $Ba(La_{0.99}Ce_{0.01})_2Si_2S_8$ phosphor (black line) and curve-fitting (red line) under 420 nm excitation and monitored at 471 nm.

the SI. The corresponding luminescence decay lifetime value can be calculated to be 34.93, 32.33, and 30.41 ns, using the first-order exponential equation.[45]

$$I = I_0 \exp\left(\frac{-t}{\tau}\right) \quad (8)$$

where I and I_0 are the luminescence intensities at time t and 0, respectively, and τ is the decay lifetime. The lifetime of Ce^{3+} in $Ba(La_{1-x}Ce_x)_2Si_2S_8$ is in the range of nanosecond, which is also reasonable for the 5d–4f transitions of Ce^{3+}[46] and similar to that usually observed[47−49] (see Table S1 in SI). With increasing Ce^{3+} concentration, both the energy transfer rate between Ce^{3+}–Ce^{3+} and the probability of energy transfer to quenching sites increase and, as a result, the lifetime shortened with the increasing Ce^{3+} concentration. However, due to the longer La–La distance (~5.5 Å) in $Ba(La_{1-x}Ce_x)_2Si_2S_8$, the low energy transfer rate between Ce^{3+} may result and, thus, a large change in the lifetime with variation of the Ce^{3+} concentration was not observed in $Ba(La_{1-x}Ce_x)_2Si_2S_8$.[44] Moreover, the well-fitting results by exponential decay with a single component illustrate that Ce^{3+} ions occupy only one site in the $BaLa_2Si_2S_8$ host, which is consistent with the Rietveld refinement of $BaLa_2Si_2S_8$:Ce^{3+} and the PL spectra shown in Table 1 and Figure 4b, respectively.

dx.doi.org/10.1021/am500483j | ACS Appl. Mater. Interfaces 2014, 6, 7260–7267

CIE Chromaticity Coordinates and Performance of LED Device Based on $Ba(La_{0.94}Ce_{0.06})_2Si_2S_8$ Phosphor. To demonstrate the potential of $Ba(La_{1-x}Ce_x)_2Si_2S_8$ for pc-WLEDs application, the $Ba(La_{0.94}Ce_{0.06})_2Si_2S_8$ phosphor was utilized to fabricate a white LED device driven by 350 mA current with red-emitting $CaAlSiN_3:Eu^{2+}$ phosphor and a 430 nm InGaN-based LED chip, as illustrated in Figure 7a. The whole visible

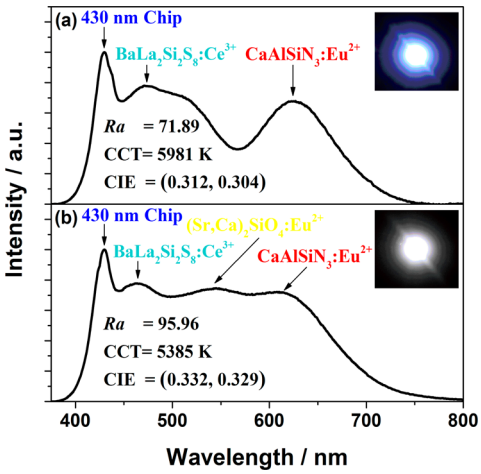

Figure 7. EL spectra of devices using (a) $Ba(La_{0.94}Ce_{0.06})_2Si_2S_8$ + red phosphor + 430 nm LED chip, (b) $Ba(La_{0.94}Ce_{0.06})_2Si_2S_8$ + red phosphor + yellow phosphor + 430 nm LED chip. The insets show the corresponding LED device photograph.

spectral region can be obtained when excited by the blue chip, and the color rendering index (R_a) of this trichromatic pc-WLED was determined to be around 72. The Commission International de l'Eclairage (CIE) chromaticity coordinates and the correlated color temperature (CCT) of the pc-WLED were measured as (x, y) = (0.312, 0.304) and 5981 K and shown in Figure 8. With the addition of proprietary yellow-emitting $(Sr,Ca)_2SiO_4:Eu^{2+}$[29] phosphor, the CRI value could be improved to 96, as illustrated in Figure 7b. The corresponding CIE chromaticity coordinates and CCT were measured to be (x, y) = (0.332, 0.329) and 5385 K, respectively. In fact, the main drawback of thiosilicate phosphors is the downgrade for high-temperature long-term operation. However, the pc-WLEDs performance can still be further ameliorated by more precise device construction, such as thermal module.

CONCLUSION

We have investigated and reported the synthesis, crystal structure, and luminescence of a unprecedented Ce^{3+}-activated thiosilicate phosphor with chemical compositions of $Ba(La_{1-x}Ce_x)_2Si_2S_8$ (x = 0.01, 0.02, 0.04, 0.06, 0.08, and 0.10). The overall luminescence performances (i.e., PL/PLE intensity, QE), decay lifetime, thermal-quenching behavior, and its application in LED fabrication were investigated. The detailed crystal structure, the morphology, and the EDS spectrum were also presented. The results show that this novel cyan-emitting phosphor can be excited over a broad range from UV to blue light and generate broadband emission. By integrating the $Ba(La_{0.94}Ce_{0.06})_2Si_2S_8$, yellow- and red-emitting phosphors on blue chip, we can obtain a warm-white-light LED device with high CRI value of 96 and CCT value of 5385 K. Our investigation results indicate that this material can potentially serve as conversion phosphors for pc-LEDs.

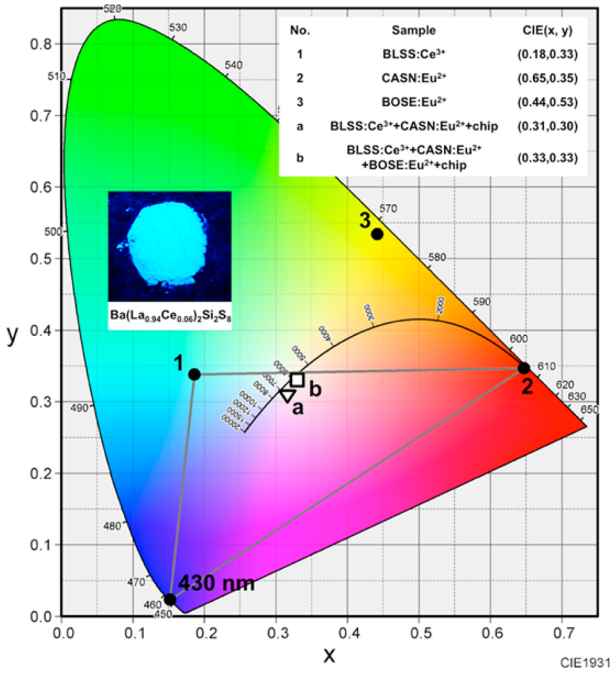

Figure 8. CIE chromaticity coordinates of $Ba(La_{0.94}Ce_{0.06})_2Si_2S_8$ phosphor and the fabricated LEDs are presented. The inset shows $Ba(La_{0.94}Ce_{0.06})_2Si_2S_8$ photo taken under 365 nm excitation.

ASSOCIATED CONTENT

Supporting Information

Further details are given in Figure S1–S3. This material is available free of charge via the Internet at http://pubs.acs.org.

AUTHOR INFORMATION

Corresponding Author

*E-mail: tmchen@mail.nctu.edu.tw.

Notes

The authors declare no competing financial interest.

ACKNOWLEDGMENTS

This research was supported by Ministry of Science and Technology of Taiwan (ROC) under Contract no. NSC101-2113-M-009-021-MY3. We thank Hung-Yu Hsu, Hsin-Han Liu, Hsin-Chieh Huang, and Chia-Wen Wang for assistance in the helpful suggestions.

REFERENCES

(1) Pimputkar, S.; Speck, J. S.; DenBaars, S. P.; Nakamura, S. Prospects for LED Lighting. *Nat. Photonics* **2009**, *3*, 179–181.

(2) Hashimoto, T.; Wu, F.; Speck, J. S.; Nakamura, S. A GaN Bulk Crystal with Improved Structural Quality Grown by the Ammonothermal Method. *Nat. Mater.* **2007**, *6*, 568–571.

(3) Robbins, D. J. The Effects of Crystal Field and Temperature on the Photoluminescence Excitation Efficiency of Ce^{3+} in YAG. *J. Electrochem. Soc.: Solid-State Sci. Technol.* **1979**, *126*, 1550–1555.

(4) Sun, C. C.; Chien, W. T.; Moreno, I.; Hsieh, C. T.; Lin, M. C.; Hsiao, S. L. Calculating Model of Light Transmission Efficiency of the Diffusers Attached to a Lighting Cavity. *Opt. Express* **2010**, *18*, 6137–6148.

(5) Moreno, I.; Sun, C. C. Modeling the Radiation Pattern of LEDs. *Opt. Express* **2008**, *16*, 1808–1819.

(6) Setlur, A. A.; Heward, W. J.; Hannah, M. E.; Happek, U. Incorporation of Si^{4+}–N^{3-} into Ce^{3+}-Doped Garnets for Warm White LED Phosphors. *Chem. Mater.* **2008**, *20*, 6277–6283.

(7) Kasuya, R.; Kawano, A.; Isobe, T.; Kuma, H.; Katano, J. Characteristic Optical Properties of Transparent Color Conversion Film Prepared from YAG:Ce^{3+} Nanoparticles. *Appl. Phys. Lett.* **2007**, *91*, 1119161−1119163.
(8) Mueller-Mach, R.; Mueller, G.; Krames, M. R.; Hoppe, H. A.; Stadker, F.; Schinick, W.; Juestel, T.; Schmidt, P. Highly Efficient All-Nitride Phosphor-Converted White Light Emitting Diode. *Phys. Status Solidi A* **2005**, *202*, 1727−1732.
(9) Xie, R. J.; Hirosaki, N.; Suehiro, T.; Xu, F. F.; Mitomo, M. A Simple, Efficient Synthetic Route to $Sr_2Si_5N_8$:Eu^{2+}-Based Red Phosphors for White Light-Emitting Diodes. *Chem. Mater.* **2006**, *18*, 5578−5583.
(10) Piao, X.; Machida, K. I.; Horikawa, T.; Hanzawa, H.; Shimomura, Y.; Kijima, N. Preparation of $CaAlSiN_3$:Eu^{2+} Phosphors by the Self-Propagating High-Temperature Synthesis and Their Luminescent Properties. *Chem. Mater.* **2007**, *19*, 4592−4599.
(11) Li, Y. Q.; Hirosaki, N.; Xie, R. J.; Takeda, T.; Mitomo, M. Yellow-Orange-Emitting $CaAlSiN_3$:Ce^{3+} Phosphor: Structure, Photoluminescence, and Application in White LEDs. *Chem. Mater.* **2008**, *20*, 6704−6714.
(12) Van Haecke, J. E.; Smet, P. F.; Poelman, D. The Influence of Source Powder Composition on the Electroluminescence of $Ca_{1-x}Sr_xS$:Eu Thin Films. *Spectrochim. Acta, Part B* **2004**, *59*, 1759−1764.
(13) Kumar, V.; Pitale, S. S. Luminescence Investigations of Ce^{3+} Doped CaS Nanophosphors. *J. Alloys Compd.* **2010**, *492*, L1−L8.
(14) Van Haecke, J. E.; Smet, P. F.; Poelman, D. Luminescent Characterization of $CaAl_2S_4$:Eu Powder. *J. Lumin.* **2007**, *126*, 508−514.
(15) Petrykin, V.; Kakihana, M. Direct Synthesis of $BaAl_2S_4$:Eu^{2+} Blue Emission Phosphor by One-Step Sulfurization of Highly Homogeneous Oxide Precursor Prepared via a Solution-Based Method. *Chem. Mater.* **2008**, *20*, 5128−5130.
(16) Li, D.; Clark, B. L.; Keszler, D. A. Color Control in Sulfide Phosphors: Turning up the Light for Electroluminescent Displays. *Chem. Mater.* **2000**, *12*, 268−270.
(17) Vecht, A.; Gibbons, C.; Davies, D.; Jing, X.; Marsh, P.; Ireland, T.; Silver, J.; Newport, A.; Barber, D. Engineering Phosphors for Field Emission Displays. *J. Vac. Sci. Technol., B* **1999**, *17*, 750−757.
(18) Jia, D.; Wang, X. J. Alkali Earth Sulfide Phosphors Doped with Eu^{2+} and Ce^{3+} for LEDs. *Opt. Mater.* **2007**, *30*, 375−379.
(19) Kuo, T. W.; Liu, W. R.; Chen, T. M. High Color Rendering White Light-Emitting Diodes Illuminator Using the Red-Emitting Eu^{2+}-Activated CaZnOS Phosphors Excited by Blue LED. *Opt. Express* **2010**, *18*, 8187−8192.
(20) Yu, R.; Wang, J.; Zhang, J.; Yuan, H.; Su, Q. Luminescence Properties of Eu^{2+}- and Ce^{3+}-Doped $CaAl_2S_4$ and Application in White LEDs. *J. Solid State Chem.* **2008**, *181*, 658−663.
(21) Parmentier, A. B.; Smet, P. F.; Bertram, F.; Christen, J.; Poelman, D. Structure and Luminescence of $(Ca,Sr)2SiS_4$: Eu^{2+} Phosphors. *J. Phys. D: Appl. Phys.* **2010**, *43*, 085401−085407.
(22) Dorenbos, P. The 5d Level Positions of the Trivalent Lanthanides in Inorganic Compounds. *J. Lumin.* **2000**, *91*, 155−176.
(23) Gai, S.; Yang, P.; Li, X.; Li, C.; Wang, D.; Dai, Y.; Lin, J. Monodisperse CeF_3, CeF_3:Tb^{3+}, and CeF_3:Tb^{3+}@LaF_3 Core/ Shell Nanocrystals: Synthesis and Luminescent Properties. *J. Mater. Chem.* **2011**, *21*, 14610−14615.
(24) Li, Y. Q.; Hirosaki, N.; Xie, R. J.; Takeda, T.; Mitomo, M. Yellow-Orange-Emitting $CaAlSiN_3$:Ce^{3+} Phosphor: Structure, Photoluminescence, and Application in White LEDs. *Chem. Mater.* **2008**, *20*, 6704−6714.
(25) Le Toquin, R.; Cheetham, A. K. Red-Emitting Cerium-Based Phosphor Materials for Solid-State Lighting Applications. *Chem. Phys. Lett.* **2006**, *423*, 352−356.
(26) Im, W. B.; Fellows, N. N.; DenBaars, S. P.; Seshadri, R.; Kim, Y. I. LaSr2AlO5, A Versatile Host Compound for Ce^{3+}-Based Yellow Phosphors: Structural Tuning of Optical Properties and Use in Solid-State White Lighting. *Chem. Mater.* **2009**, *21*, 2957−2966.
(27) Shimomura, Y.; Kurushima, T.; Kijima, N. Photoluminescence and Crystal Structure of Green-Emitting Phosphor $CaSc_2O_4$:Ce^{3+}. *J. Electrochem. Soc.* **2007**, *154*, J234−J238.
(28) Gulay, L. D.; Daszkiewicz, M.; Ruda, I. P.; Marchuk, O. V. $La_2Pb(SiS_4)_2$. *Acta Crystallogr., Sect. C* **2010**, *C66*, i19−i21.
(29) Luo, X. X.; Cao, W. H.; Sun, F. The Development of Silicate Matrix Phosphors with Broad Excitation Band for Phosphor-Converted White LED. *Chin. Sci. Bull.* **2008**, *53*, 2923−2930.
(30) Uheda, K.; Hirosaki, N.; Yamamoto, Y.; Naito, A.; Nakajima, T.; Yamamoto, H. Luminescence Properties of a Red Phosphor, $CaAlSiN_3$:Eu^{2+}, for White Light-Emitting Diodes. *Electrochem. Solid-State Lett.* **2006**, *9*, H22−H25.
(31) Larson, A. C.; Von Dreele, R. B. General Structure Analysis System (GSAS). *Los Alamos National laboratory Report LAUR* **2000**, 86−748.
(32) Toby, B. H. EXPGUI, A Graphical User Interface for GSAS. *J. Appl. Crystallogr.* **2001**, *34*, 210−213.
(33) Shannon, R. D. Revised Effective Ionic Radii and Systematic Studies of Interatomic Distances in Halides and Chalcogenides. *Acta Crystallogr., Sect. A* **1976**, *32*, 751−767.
(34) Daszkiewicza, M.; Marchukb, O. V.; Gulayc, L. D.; Kaczorowski, D. Crystal Structures and Magnetic Properties of $R_2PbSi_2S_8$ (R = Y, Ce, Pr, Nd, Sm, Gd, Tb, Dy, Ho), $R_2PbSi_2Se_8$ (R = La, Ce, Pr, Nd, Sm, Gd) and $R_2PbGe_2S_8$ (R = Ce, Pr) Compounds. *J. Alloys Compd.* **2012**, *519*, 85−91.
(35) Kubelka, P.; Munk, F. Ein Beitrag zur Optik der Farbanstriche. *Z. Technol. Phys. (Leipzig)* **1931**, *12*, 593−601.
(36) Wu, Y. C.; Wang, D. Y.; Chen, T. M.; Lee, C. S.; Chen, K. J.; Kuo, H. C. A Novel Tunable Green- to Yellow-Emitting β-YFS:Ce^{3+} Phosphor for Solid-State Lighting. *ACS Appl. Mater. Interfaces* **2011**, *3*, 3195−3199.
(37) Kodama, N.; Yamaga, M.; Henderson, B. Energy Levels and Symmetry of Ce^{3+} in Fluoride and Oxide Crystals. *J. Appl. Phys.* **1998**, *84*, 5820−5822.
(38) Blasse, G. Energy Transfer in Oxidic Phosphors. *Philips Res. Rep.* **1969**, *24*, 131−144.
(39) Shang, M. M.; Li, G. G.; Kang, X. J.; Yang, D. M.; Geng, D. L.; Lin, J. Tunable Luminescence and Energy Transfer Properties of Sr_3AlO_4F:RE^{3+} (RE = Tm/Tb, Eu, Ce) Phosphors. *ACS Appl. Mater. Interfaces* **2011**, *3*, 2738−2746.
(40) Dexter, D. L. A Theory of Sensitized Luminescence in Solids. *J. Chem. Phys.* **1953**, *21*, 836−850.
(41) Van Uitert, L. G. Characterization of Energy Transfer Interactions between Rare Earth Ions. *J. Electrochem. Soc.* **1967**, *114*, 1048−1053.
(42) Mello, J. C.; Wittmann, H. F.; Friend, R. H. An Improved Experimental Determination of External Photoluminescence Quantum Efficiency. *Adv. Mater.* **1997**, *9*, 230−232.
(43) Wang, D. Y.; Huang, C. H.; Wu, Y. C.; Chen, T. M. $BaZrSi_3O_9$:Eu^{2+}: A Cyan-Emitting Phosphor with High Quantum Efficiency for White Light-Emitting Diodes. *J. Mater. Chem.* **2011**, *21*, 10818−10822.
(44) Xie, R. J.; Hirosaki, N.; Kimura, N.; Sakuma, K.; Mitomo, M. 2-Phosphor-Converted White Light-Emitting Diodes Using Oxynitride/ Nitride Phosphors. *Appl. Phys. Lett.* **2007**, *90*, 191101−191103.
(45) Pang, R.; Li, C.; Shi, L.; Su, Q. A Novel Blue-Emitting Long-Lasting Proyphosphate Phosphor $Sr_2P_2O_7$:Eu^{2+},Y^{3+}. *J. Phys. Chem. Solids* **2009**, *70*, 303−306.
(46) Blasse, G.; Grabmaier, B. C. *Luminescent Materials*; Springer: Berlin, 1994; p 675.
(47) Huang, C. H.; Chen, T. M. A Novel Single-Composition Trichromatic White-Light $Ca_3Y(GaO)_3(BO_3)_4$:Ce^{3+},Mn^{2+}, Tb^{3+} Phosphor For UV-LED. *J. Phys. Chem. C* **2011**, *115*, 2349−2355.
(48) Bachmann, V.; Ronda, C.; Meijerink, A. Temperature Quenching of Yellow Ce^{3+} Luminescence in YAG:Ce. *Chem. Mater.* **2009**, *21*, 2077−2084.
(49) Liu, Y.; Hao, J.; Zhuang, W.; Hu, Y. Structural and Luminescent Properties of Gel-combustion Synthesized Green-emitting

$Ca_3Sc_2Si_3O_{12}:Ce^{3+}$ Phosphor for Solid-State Lighting. *J. Phys. D: Appl. Phys.* **2009**, *42*, 245102−245108.